Phys. Status Solidi A **206**, No. 8, 1761–1765 (2009) / **DOI** 10.1002/pssa.200881588

physica status solidi a
www.pss-a.com
applications and materials science

Sensitivity of triple-crystal X-ray diffractometers to microdefects in silicon

V. B. Molodkin, S. I. Olikhovskii, E. G. Len*, E. N. Kislovskii, V. P. Kladko, O. V. Reshetnyk, T. P. Vladimirova, and B. V. Sheludchenko

G. V. Kurdyumov Institute for Metal Physics of NASU, Vernadsky Blvd. 36, 03680 Kyiv, Ukraine

Received 17 September 2008, revised 5 December 2008, accepted 5 March 2009
Published online 20 July 2009

PACS 61.05.cc, 61.05.cp, 61.72.Dd

* Corresponding author: e-mail len@imp.kiev.ua, Phone: +38-044-422-95-83, Fax: +38-044-424-05-30

The dynamical theory, which describes both diffraction profiles and reciprocal space maps measured from imperfect crystals with account for instrumental factors of triple-crystal diffractometer (TCD), has been developed for adequate quantitative characterization of microdefects. Analytical expressions for coherent and diffuse scattering (DS) intensities measured by TCD in the Bragg diffraction geometry have been derived by using the generalized statistical dynamical theory of X-ray scattering in real single crystals with randomly distributed defects. The DS intensity distributions from single crystals containing clusters and dislocation loops have been described by explicit analytical expressions. Particularly, these expressions take into account anisotropy of displacement fields around defects with discrete orientations. Characteristics of microdefect structures in silicon single crystals grown by Czochralsky- and float-zone methods have been determined by analyzing the measured TCD profiles and reciprocal space maps. The sensitivities of reciprocal space maps and diffraction profiles to defect characteristics have been compared.

1 Introduction The experiments with using triple-crystal X-ray diffractometer (TCD) provide the most complete diffractometric characterization of both defects in crystal bulk and strains in disturbed subsurface layers but there exist some experimental and theoretical difficulties in the triple-crystal X-ray diffractometry for the maximal realization of its potentialities. First, it is often necessary to find a compromise between diffractometer resolution and luminosity for optimizing the diagnostic capability of measurements. Second, at quantitative determination of defect characteristics in single and multilayered crystal structures, one needs for adequate theoretical models of diffraction experiments.

On the one hand, the most widely used variants of the diffraction theory like Kato's statistical dynamical theory [1–5] do not give evident and direct relationships between defect characteristics and parameters of diffraction intensity distributions. Thus, the reliable information on defect characteristics cannot be extracted from measured diffraction patterns by using results of such theories. On the other hand, when performing TCD measurements of the diffuse scattering (DS) intensity distributions, the consideration is usually restricted to the analysis only in those reciprocal lattice regions where the coherent component of the diffraction intensity can be neglected or subtracted by using the equations for perfect crystals. But such approach can lead to systematic errors when determining the characteristics of imperfections, especially, large microdefects which produce DS peaks commensurable in width and height, and angular positions with coherent ones.

The consecutive account for dynamical effects in both coherent and DS components has been carried out in the generalized dynamical theory of X-ray scattering by imperfect crystals with randomly distributed microdefects [6, 7]. The main advantage of this theory is the availability of self-consistent analytical expressions for coherent and DS intensities and their direct relations with defect characteristics, which provides the unique possibility to perform the full quantitative characterization of defect structures.

It should be mentioned here that in kinematical diffraction cases the use of the dynamical formulas remains valid as well. Moreover, if the dynamical approach is used, it is not necessary to analyze and justify its applicability for each specific experiment, what is required for the kinematical consideration.

The purpose of the present article is obtaining the analytical expressions for the description of both total diffraction profiles and reciprocal space maps measured by TCD in the Bragg diffraction geometry with account for DS contributions from various-type microdefects including dislocation loops with discrete orientations. The analytical expressions for coherent and DS components of the imperfect crystal reflectivity measured by TCD will be derived in Section 2. The characterization of different defect structures in silicon crystals by using maps of DS intensity and total TCD profiles as well as a comparison of these diffractometric methods will be given in Section 3.

2 Diffraction model The intensity registered by TCD detector from investigated imperfect crystal can be represented in the form [8, 9]:

$$I\left(\Delta\theta, \Delta\theta'\right) = I_{\rm coh}\left(\Delta\theta,\ \Delta\theta'\right) + I_{\rm diff}\left(\Delta\theta, \Delta\theta'\right). \qquad (1)$$

This intensity depends only on two angular variables, namely, deviations of investigated crystal $\Delta\theta$ and analyzer crystal $\Delta\theta'$ from their exact reflecting positions.

2.1 Coherent component In the case of dispersionless $(n, -n, n)$ geometry, considered here for simplicity, the coherent component of the intensity measured by TCD has the form [8, 9]:

$$I_{\rm coh}\left(\Delta\theta, \Delta\theta'\right) = I_0 \int_{-\infty}^{\infty} {\rm d}x\, R_{\rm M}^{n_{\rm M}}\left(b_{\rm M}^{-1}\left[b_{\rm S}^{-1}(x-\Delta\theta) - \Delta\theta\right]\right) \times R_{\rm coh}\left(b_{\rm S}^{-1}(x-\Delta\theta)\right) R_{\rm A}^{n_{\rm A}}\left(x - \Delta\theta'\right), \qquad (2)$$

where I_0 is an intensity of incident X-ray beam, $R_{\rm M}$ and $R_{\rm A}$ are reflection coefficients of the monochromator and analyzer crystals (which can contain microdefects in bulk and strains in surface layers), $n_{\rm M}$ and $n_{\rm A}$ are numbers of reflections at these crystal, $b_{\rm M}$ and $b_{\rm S}$ are asymmetry parameters of monochromator and sample crystals, respectively, $b = \gamma_0|\gamma_{\boldsymbol{H}}|^{-1}$ (subscripts M and S are omitted), $\gamma_0 = \sin(\theta_{\rm B} - \psi)$ and $\gamma_{\boldsymbol{H}} = -\sin(\theta_{\rm B} + \psi)$ are direction cosines with respect to the inner normal $\boldsymbol{n}$ to the entrance crystal surface for wave vectors of an incident plane wave $\boldsymbol{K}$ and a scattered plane wave $\boldsymbol{K}' = \boldsymbol{K} + \boldsymbol{H}$, respectively, $\boldsymbol{H}$ is a reciprocal lattice vector, $\theta_{\rm B}$ is the Bragg angle, ψ is an angle between crystal surface and reflecting planes. The expressions for the coherent component of reflection coefficient $R_{\rm coh}(\Delta\theta)$ for imperfect crystal have been derived in Ref. [6]. They take into account all effects of dynamical scattering including extinction of Bragg waves due to DS on microdefects. The attenuation of Bragg waves, which is caused by the coefficient of absorption due to DS [6, 7], is in general substantially more essential than that caused by the static Debye–Waller factor. Thus, unlike kinematic theory [10], the dynamical coherent scattering is not less sensitive to defect characteristics than DS.

2.2 Diffuse component The diffuse component of the intensity measured by TCD can be represented by the expression [8, 9]:

$$I_{\rm diff}\left(\Delta\theta, \Delta\theta'\right) = I_0 \int_{-\infty}^{\infty} {\rm d}x R_{\rm M}^{n_{\rm M}}(x) \times \int_{-\infty}^{\infty} {\rm d}x' r_{\rm diff}(\boldsymbol{p}) R_{\rm A}^{n_{\rm A}}\left(x' - \Delta\theta'\right). \qquad (3)$$

The function $r_{\rm diff}\ (\boldsymbol{p})$ in Eq. (3) represents the diffuse component of the differential reflection coefficient $R_{\rm D}(\boldsymbol{k})$ [6, 7] integrated over a vertical divergence

$$r_{\rm diff}\ (\boldsymbol{p}) = K^{-1} \int {\rm d}k_y R_{\rm D}\ (\boldsymbol{k}), \qquad (4)$$

$$\boldsymbol{p} = \boldsymbol{q} - k_y \boldsymbol{e}_y,\ \ \boldsymbol{q} = \boldsymbol{k} + i\mu_{\rm i}\boldsymbol{n}. \qquad (5)$$

In Eq. (5), the complex momentum transfer $\boldsymbol{q}$ enclose the interference absorption coefficient $\mu_{\rm i}$, $K = |\boldsymbol{K}| = 2\pi/\lambda$, λ is X-ray wave length. Components k_x and k_z of the vector $\boldsymbol{k} = (k_x, k_y, k_z)$ are in the plane of coherent scattering $(\boldsymbol{K}, \boldsymbol{H})$. The component k_z is directed along the normal $\boldsymbol{n}$, and vector $\boldsymbol{k}$ describes deviation of the wave vector $\boldsymbol{K}'$ from the reciprocal lattice point H, which corresponds to the reciprocal lattice vector $\boldsymbol{H}$.

When several types of microdefects are present in a crystal simultaneously, but without mutual correlation, Eq. (4) should be simply replaced by the sum of corresponding expressions for each type of defects [11]. After integrating in Eq. (4) over a vertical divergence k_y with account for Eq. (5) we obtain in the Huang scattering region $\left(k_y \le k_y^{{\rm m}\alpha} \equiv \sqrt{k_{{\rm m}\alpha}^2 - p^2}\right.$, where $p \equiv |\boldsymbol{p}|$, $k_{{\rm m}\alpha} \equiv 1/R_{\rm eff}^{\alpha}$, and $\left.R_{\rm eff}^{\alpha}\right.$ is an effective radius of α type defect [9]$\left.\right)$:

$$r_{\rm diff}\ (\boldsymbol{p}) = K\pi^{-1} \sum_{\alpha} M_{\alpha}\left(I_{{\rm SW}\,\alpha}^{\infty} - I_{{\rm SW}\,\alpha}^{k_y^{{\rm m}\alpha}} + I_{{\rm H}\,\alpha}^{k_y^{{\rm m}\alpha}}\right), \qquad (6)$$

$$M_{\alpha} = c_{\alpha} m_0 C^2 E^2 \left(2\gamma_0\mu_{\rm i}\right)^{-1},\ \ m_0 = \pi\, v_{\rm c} \frac{\left(H\,|\chi_{{\rm r}\boldsymbol{H}}|/\lambda\right)^2}{4},$$

where c_{α} is a concentration of randomly distributed α-type defects per one lattice site, polarization factor $C = 1$ or $\cos(2\theta_{\rm B})$ for σ and π polarization states, respectively, $v_{\rm c}$ is the volume of unit cell, $H = |\boldsymbol{H}|$, E is the static Debye–Waller factor, $\chi_{{\rm r}\boldsymbol{H}}$ is a Fourier component of the real part of the complex crystal polarizability.

Similarly, in the Stokes–Wilson scattering region ($k_y > k_y^{m\alpha}$) we obtain:

$$r_{\text{diff}}(p) = K\pi^{-1}\sum_{\alpha} M_\alpha I^{\infty}_{\text{SW}\,\alpha}. \tag{7}$$

In Eqs. (6) and (7), the quantities $I^{k_y^m}_{\text{SW}\,\alpha}$ and $I^{k_y^m}_{\text{H}\,\alpha}$ represent the following integrals (with limits $k_y^m = k_y^{m\alpha}$ or ∞) over Huang and Stokes–Wilson scattering regions, respectively:

$$I^{k_y^m}_{\text{H}\,\alpha} = \int_{-k_y^m}^{k_y^m} \mathrm{d}k_y F_{\text{H}\,\alpha}, \quad F_{\text{H}\,\alpha} = \left\langle \left| H_0 u_{\alpha \boldsymbol{q}} \right|^2 \right\rangle, \tag{8}$$

$$I^{k_y^m}_{\text{SW}\,\alpha} = \int_{-k_y^m}^{k_y^m} \mathrm{d}k_y F_{\text{SW}\,\alpha}, \quad F_{\text{SW}\,\alpha} = \left(\frac{k^2_{\text{m}\alpha}}{q^2}\right) F_{\text{H}\,\alpha}, \tag{9}$$

where $u_{\alpha \boldsymbol{q}}$ are the Fourier components of static displacements fields from α type defect [10], $\boldsymbol{H}_0 = \boldsymbol{H}/H$, angle brackets $\langle \cdots \rangle$ denote the averaging over discrete orientations of defects. After averaging and integration over k_y in Eqs. (8) and (9) we obtain:

$$I^{\infty}_{\text{SW}\alpha} = \frac{k^2_{\text{m}\alpha}\pi}{2p^3}\left\{B_{1\alpha} + \frac{3}{4}\left[B_{2\alpha} + \frac{5}{6}\left(B_{3\alpha} + \frac{7}{8}B_{4\alpha}\right)\right]\right\}, \tag{10}$$

$$\begin{aligned} I^{k_y^{m\alpha}}_{\text{SW}\,\alpha} &= \frac{k^2_{\text{m}\alpha}}{p^3}\left\{B_{1\alpha} + \frac{3}{4}\left[B_{2\alpha} + \frac{5}{6}\left(B_{3\alpha} + \frac{7}{8}B_{4\alpha}\right)\right]\right\} \\ &\times \left(\arctan\left(\frac{k_y^{m\alpha}}{p}\right) + \frac{k_y^{m\alpha} p}{k^2_{\text{m}\alpha}}\right) \\ &+ \frac{k_y^{m\alpha}}{2k^2_{\text{m}\alpha}}\left[B_{2\alpha} + \frac{3}{4}\left(B_{3\alpha} + \frac{5}{6}B_{4\alpha}\right)\right] \\ &+ \frac{k_y^{m\alpha} p^2}{3k^4_{\text{m}\alpha}}\left(B_{3\alpha} + \frac{5}{6}B_{4\alpha}\right) + \frac{k_y^{m\alpha} p^4}{4k^6_{\text{m}\alpha}}B_{4\alpha}, \end{aligned} \tag{11}$$

$$\begin{aligned} I^{k_y^{m\alpha}}_{\text{H}\,\alpha} &= \frac{1}{p}\left\{2B_{1\alpha} + \left[B_{2\alpha} + \frac{3}{4}\left(B_{3\alpha} + \frac{5}{6}B_{4\alpha}\right)\right]\right\} \\ &\times \arctan\left(\frac{k_y^{m\alpha}}{p}\right) + \frac{k_y^{m\alpha}}{k^2_{\text{m}\alpha}}\left[B_{2\alpha} + \frac{3}{4}\left(B_{3\alpha} + \frac{5}{6}B_{4\alpha}\right)\right] \\ &+ \frac{k_y^{m\alpha} p^2}{2k^4_{\text{m}\alpha}}\left(B_{3\alpha} + \frac{5}{6}B_{4\alpha}\right) + \frac{k_y^{m\alpha} p^4}{3k^6_{\text{m}\alpha}}B_{4\alpha}. \end{aligned} \tag{12}$$

In the case of spherical clusters ($\alpha = 1$), the coefficients $B_{i\alpha}$ ($i = \overline{1,4}$) in Eqs. (10)–(12) take the following values:

$$B_{01} = \left(\frac{4\pi A_{\text{C}}}{v_{\text{c}}}\right)^2, \tag{13}$$

$$\begin{aligned} B_{11} &= B_{01}H^2_{0y}, \; B_{21} = B_{01}\left(\left|\boldsymbol{H}_0\boldsymbol{p}_0\right|^2 - H^2_{0y}\right), \\ B_{31} &= B_{41} = 0, \end{aligned}$$

where $A_{\text{C}} = \Gamma\varepsilon R_1^3$ is the cluster strength, $\Gamma = (1+\nu)/(3-3\nu)$, ε is the strain at the cluster boundary, ν is the Poisson ratio, R_1 is the radius of spherical cluster, $\boldsymbol{p}_0 = \boldsymbol{p}/p$.

In the case of dislocation loops ($\alpha = 2$) with discrete orientations $\langle 110 \rangle$ or $\langle 111 \rangle$, the coefficients B_{i2} take the form:

$$B_{02} = 4C^2_{n_1}\frac{\left[A_{\text{L}}/n_1 v_{\text{c}}(1-\nu)\right]^2}{3}, \tag{14}$$

$$\begin{aligned} B_{12} &= B_{02}\left\{4(1-\nu)^2 + \left[(4\beta(1-n_1)-3)\nu^2\right.\right. \\ &\left.\left. + (2\beta(n_1-2)+8)\nu + \beta - 4\right]H^2_{0y}\right\}, \end{aligned}$$

$$\begin{aligned} B_{22} &= B_{02}\left\{\left[(9-4\beta n_1)\nu^2 + 2(\beta n_1 - 6)\nu + \beta + 4\right]\right. \\ &\times \left|\boldsymbol{H}_0\boldsymbol{p}_0\right|^2 + 4(1-\nu)\left[(\beta-3)\left(2H^2_{0y} + (1-\nu)\right.\right. \\ &\left.\left.\times S\left(\boldsymbol{H}_0, \boldsymbol{H}_0, \boldsymbol{p}_0, \boldsymbol{p}_0^*\right)\right) - 2\text{Re}\left(\boldsymbol{H}_0\boldsymbol{p}_0\right)^2\right] \\ &+ \left[(4\beta(n_1-1)+3)\nu^2 - 2(\beta(n_1-4)+10)\nu\right. \\ &\left.\left. - 7\beta + 22\right]H^2_{0y}\right\}, \end{aligned}$$

$$\begin{aligned} B_{32} &= B_{02}(\beta-3)\left\{\left(3 + S\left(\boldsymbol{p}_0, \boldsymbol{p}_0, \boldsymbol{p}_0^*, \boldsymbol{p}_0^*\right)\right)H^2_{0y} - 2\left|\boldsymbol{H}_0\boldsymbol{p}_0\right|^2\right. \\ &\left. - 4(1-\nu)\left(1 + \text{Re}\left[\left(\boldsymbol{H}_0\boldsymbol{p}_0\right)S\left(\boldsymbol{H}_0, \boldsymbol{p}_0, \boldsymbol{p}_0, \boldsymbol{p}_0^*\right)\right]\right)\right\}, \end{aligned}$$

$$\begin{aligned} B_{42} &= B_{02}(\beta-3)\left(\left|\boldsymbol{H}_0\boldsymbol{p}_0\right|^2 - H^2_{0y}\right) \\ &\times \left(1 + S\left(\boldsymbol{p}_0, \boldsymbol{p}_0, \boldsymbol{p}_0^*, \boldsymbol{p}_0^*\right)\right), \end{aligned}$$

$$\begin{aligned} S(\boldsymbol{a}_1, \boldsymbol{a}_2, \boldsymbol{a}_3, \boldsymbol{a}_4) &= a_{1x}a_{2x}a_{3x}a_{4x} + a_{1y}a_{2y}a_{3y}a_{4y} \\ &+ a_{1z}a_{2z}a_{3z}a_{4z}, \end{aligned}$$

where $A_{\text{L}} = \pi|\boldsymbol{b}|R_2^2$ is the dislocation loop strength, R_2 is the radius of dislocation loop, $\beta = C^1_{n_1}/C^2_{n_1}$, C^m_n are binomial coefficients, n_1 is the number of units in the Burgers vector $\boldsymbol{b}$, the pair of numbers (n_1, β) in the last formulas denotes the type of averaging, and for $\langle 110 \rangle$ and $\langle 111 \rangle$ orientations of dislocation loops takes the values (2,2) and (3,1), respectively.

The interference absorption coefficient μ_{i} in Eqs. (5)–(12) plays a role of the cut parameter and removes the divergence at $(k_x, k_z) \to 0$. This coefficient allows to describe correctly the contribution of diffuse component to TCD diffraction profiles in the region of coherent peak, where this contribution is rapidly decreased (approximately by an order of magnitude) because μ is increased from the value μ_0 (linear coefficient of photoelectric absorption) to the value of $2\pi/\Lambda$ (Λ is an extinction length).

It should be emphasized that the analytical results obtained for discrete oriented dislocation loops can be immediately use in the case of disc-shaped clusters lying in corresponding crystal lattice planes. This can be made through changing in coefficients B_{i2} the vector $\boldsymbol{b}$ to the unit normal to these planes and by replacing the dislocation loop strength A_L in Eq. (14) by the cluster strength $A_C = 3\Gamma\varepsilon V_C/4\pi$ (where V_C is the volume of a disc-shaped cluster).

3 Analysis of measurements With using the above formulas (1)–(12), the different defect structures in single silicon crystals grown by float zone (FZ Si) and Czochralsky (Cz Si) methods have been investigated by analyzing reciprocal space maps, which were measured by commercial diffractometer PAN analytical X'Pert Pro MRD XL, and diffraction profiles, which were measured with a higher resolution by homemade TCD [8, 9].

As can be seen in Fig. 1, the map allowing reliable defect characterization was measured only from annealed Cz Si sample (50 h at 1150 °C) with well-developed microdefect structure (Fig. 1a). For this sample, the characterization results obtained from the map coincide sufficiently well for predominant type of defects (large dislocation loops) with those obtained from the set of diffraction profiles one of which is shown in Fig. 1c. Some discrepancy in the concentration (see Table 1) can be explained by the presence of smaller dislocation loops and oxygen precipitates, which also give contributions to the diffraction pattern but cannot be distinguished by the commercial diffractometer because of insufficient resolution ability. The characterization of small clusters and two types of small dislocation loops was possible due to using the set of diffraction profiles measured by homemade diffractometer. Exclusively important factor for the reliable determination of characteristics of these defects was the use of the developed dynamical theory, which permits determining simultaneously a set of defect characteristics due to the self-consistent consideration of both diffuse and coherent components of diffraction patterns.

It should be remarked that the weak asymmetry along Q_z axis, which is observed in measured maps from Cz Si sample, can be caused by the antisymmetric part of DS intensity from microdefects [10], but was not taken into account in the performed calculations.

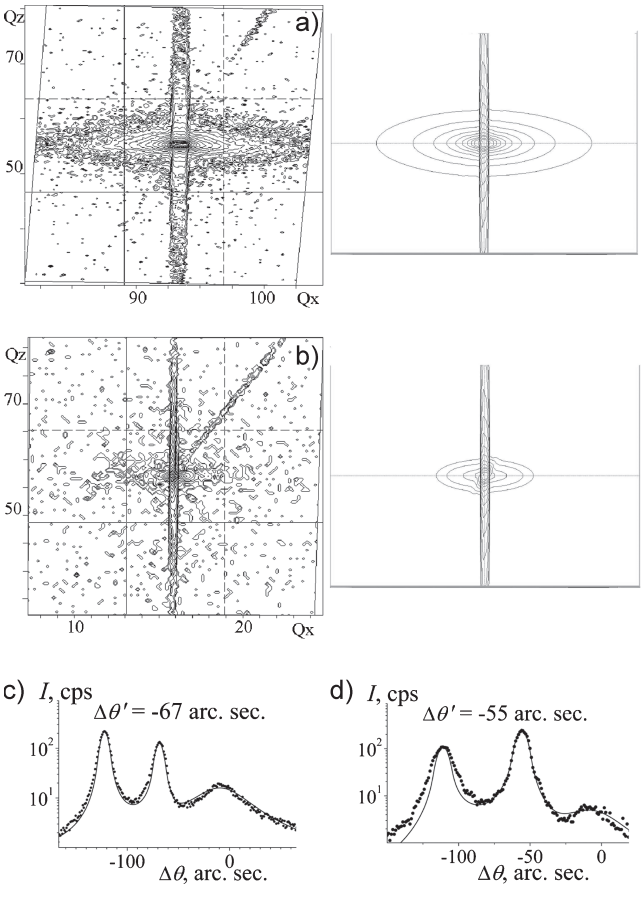

Figure 1 Reciprocal space maps (left – measured by commercial diffractometer, right – calculated) and total TCD profiles (markers – measured by homemade diffractometer, line – calculated) from annealed Cz Si (a,c) and FZ Si (b,d) samples (111 reflection, CuKα radiation).

The map measured from as-grown FZ Si sample (Fig. 1b) shows almost perfect crystalline structure with a weak diffuse background whereas the corresponding diffraction profiles (Fig. 1d) exhibit clear diffuse peaks. These profiles provide a sufficiently reliable determination of characteristics of large dislocation loops (see Table 1). However, the observed DS intensity is too weak to distinguish the contribution from smaller loops. For solving the problem of diffractometric detection and characterization of small defects with small concentrations one should additionally use the integral

Table 1 Radii (R_α) and number densities ($n_\alpha = c_\alpha/v_c$) of spherical oxygen clusters ($\alpha = 1$) and circular dislocation loops ($\alpha = 2$) in Cz Si and FZ Si crystals obtained by fitting reciprocal space maps and total TCD profiles.

sample	data type	R_1 (nm)	n_1 (cm^{-3})	R_2 (μm)	n_2 (cm^{-3})
Cz Si	profile	10 ± 1	$1.0 \pm 0.1 \times 10^{13}$	0.05 ± 0.005	$8.0 \pm 2 \times 10^{11}$
				0.3 ± 0.03	$9.0 \pm 3 \times 10^{9}$
				5.0 ± 0.3	$4 \pm 0.5 \times 10^{7}$
	map	–	–	4.3 ± 0.6	$1.9 \pm 1 \times 10^{8}$
FZ Si	profile	–	–	1.15 ± 0.1	$3.5 \pm 1 \times 10^{8}$
	map	–	–	2.1 ± 0.5	$7.3 \pm 3 \times 10^{7}$

diffraction methods like the double-crystal diffractometry with widely open detector window, where the DS intensity is integrated over Ewald sphere [6, 7].

4 Conclusions We propose the dynamical theory which self-consistently describes both coherent and diffuse components of diffraction profiles and reciprocal space maps measured from imperfect crystals. The instrumental factors of TCD were taken into account as well. The simultaneous analysis of both coherent and diffuse components of diffraction patterns, as well as the combination of various diffractometric methods, provides the possibility for a more reliable characterization of multiparametric defect structures.

References

[1] N. Kato, Acta Crystallogr. A **36**, 763; 770 (1980); Acta Crystallogr. A **47**, 1 (1991).

[2] V. Holý and K. T. Gabrielyan, Phys. Status Solidi B **140**, 39 (1987).

[3] V. A. Bushuev, Sov. Phys. Crystallogr. **34**, 163 (1989).

[4] J. P. Guigay and F. N. Chukhovskii, Acta Crystallogr. A **48**, 819 (1992); Acta Crystallogr. A **51**, 288 (1995).

[5] K. M. Pavlov and V. I. Punegov, Acta Crystallogr. A **56**, 227 (2000).

[6] V. B. Molodkin, S. I. Olikhovskii, E. N. Kislovskii, E. G. Len, and E. V. Pervak, Phys. Status Solidi B **227**, 429 (2001).

[7] S. I. Olikhovskii, V. B. Molodkin, E. N. Kislovskii, E. G. Len, and E. V. Pervak, Phys. Status Solidi B **231**, 199 (2002).

[8] S. I. Olikhovskii, V. B. Molodkin, Ye. M. Kislovskii, O. V. Reshetnyk, T. P. Vladimirova, E. G. Len, G. E. Ice, R. O. Barabash, R. Köhler, and D. O. Grigoriev, Metallofiz. Noveishie Tekhnol. **27**, 947 (2005).

[9] S. I. Olikhovskii, V. B. Molodkin, E. N. Kislovskii, O. V. Reshetnyk, T. P. Vladimirova, G. E. Ice, R. I. Barabash, R. Köhler, and D. O. Grigoriev, Metallofiz. Noveishie Tekhnol. **27**, 1251 (2005).

[10] M. A. Krivoglaz, X-Ray and Neutron Scattering in Nonideal Crystals (Springer, Berlin, 1996), p. 466.

[11] E. N. Kislovskii, S. I. Olikhovskii, V. B. Molodkin, V. V. Nemoshkalenko, V. P. Krivitsky, E. G. Len, E. V. Pervak, G. E. Ice, and B. C. Larson, Phys. Status Solidi B **231**, 213 (2002).